Mutation in the β-Tubulin Signature Motif Suppresses Microtubule GTPase Activity and Dynamics, and Slows Mitosis†

Cynthia A. Dougherty,‡ Carleton R. Sage,§ Ashley Davis,‖ and Kevin W. Farrell*

Department of Molecular, Cellular and Developmental Biology, University of California, Santa Barbara, California 93106

Received January 10, 2001; Revised Manuscript Received October 8, 2001

ABSTRACT: We introduced a threonine-to-glycine point mutation at position 143 in the "tubulin signature motif" 140Gly-Gly-Gly-Thr-Gly-Ser-Gly146 of *Saccharomyces cerevisiae* β-tubulin. In an electron diffraction model of the tubulin dimer, this sequence comes close to the phosphates of a guanine nucleotide bound in the β-tubulin exchangeable E site. Both the GTP-binding affinity and the microtubule (MT)-dependent GTPase activity of tubulin isolated from haploid *tub2-T143G* mutant cells were reduced by at least 15-fold, compared to tubulin isolated from control wild-type cells. The growing and shortening dynamics of MTs assembled from αβ:Thr143Gly-mutated dimers were also strongly suppressed, compared to control MTs. The in vitro properties of the mutated MTs (slower growing and more stable) are consistent with the effects of the *tub2-T143G* mutation in haploid cells. The average length of MT spindles in large-budded mutant cells was only 3.7 ± 0.2 μm, approximately half of the size of MT arrays in large-budded wild-type cells (average length = 7.1 ± 0.4 μm), suggesting that there is a delay in mitosis in the mutant cells. There was also a higher proportion of large-budded cells with unsegregated nuclei in mutant cultures (30% versus 12% for wild-type cells), again suggesting such a delay. The results show that β:Thr143 of the tubulin signature motif plays an important role in GTP binding and hydrolysis by the β-tubulin E site and support the idea that tubulins belong to a family of proteins within the GTPase superfamily that are structurally distinct from the classic GTPases, such as EF-Tu and p21ras. The data also suggest that MT dynamics are critical for MT function in yeast cells and that spindle MT assembly and disassembly could be coordinated with other cell-cycle events by regulating β-tubulin GTPase activity.

Microtubules (MTs) participate in a variety of cellular functions, including intracytoplasmic transport, cell-shape maintenance, secretion, and chromosome movement. The diversity of the cellular roles played by MTs is paralleled by large differences in their dynamic properties, and it now seems clear that MT dynamic properties are precisely regulated for the different cellular functions that MTs perform. Two types of MT dynamic behaviors have been characterized in vitro: the unidirectional flux of tubulin subunits through MTs ("treadmilling"; *1*) and the stochastic growing and shortening of MTs ("dynamic instability"; *2*). Cytological studies have shown that MTs in cells also exhibit these dynamic properties (reviewed in ref *3*).

It has been proposed that β-tubulin GTPase activity is involved both in the treadmilling dynamics of MTs (*1*) and in MT dynamic instability (*2*). Yet, despite the apparent importance of the β-tubulin GTPase activity, structure−function studies of the exchangeable nucleotide-binding site on β tubulin (the E site) were hampered by the lack of a structural model of the tubulin αβ heterodimer. Compounding the problem was the fact that none of the tubulins showed the highly conserved primary sequence motifs that contributed to the nucleotide-binding site in classic GTPases, such as EF-Tu and p21ras (*4*).

Recently, however, an electron crystallographic model of the tubulin dimer (*5*) has made possible a more rational approach to studying the β-tubulin GTP-binding E site. In this study, we examined the role of the glycine-rich "tubulin signature motif" Gly-Gly-Gly-Thr-Gly-Ser-Gly. In the electron crystallographic model of the tubulin dimer, this loop passes close to the phosphates of the E-site nucleotide, and mutations in the cognate sequences of ATPases (*6*, *7*) and the bacterial septum GTPase FtsZ (*8*, *9*) strongly affect nucleotide binding and hydrolysis. If the β-tubulin signature motif also plays a role in GTP binding and hydrolysis, then mutations in this region should similarly affect tubulin−GTP binding and GTPase activity.

Using the single β-tubulin gene, *TUB2,* of *Saccharomyces cerevisiae,* we introduced a threonine-to-glycine point mutation into the sequence coding for the tubulin signature motif and examined its effect on tubulin−GTP binding and hydrolysis and on steady-state MT dynamics in vitro. We also examined whether the mutation affected nuclear migration and segregation during the cell cycle, both of which are MT-dependent processes. The goals were to determine whether the tubulin signature motif played a role in GTP

Table 1: *S. cerevisiae* Strains

strain	β-tubulin genotype	selection-marker genotype
FY41	*TUB2*	Mat a, Leu2d1, Trp1d63, Ura3−52, His4−917
YT143G	*tub2*-T143G	Mat a, Leu2d1, Trp1d63, URA3, His4−917

binding and hydrolysis and whether altering tubulin GTPase activity led to changes in the dynamic properties of MTs and their cellular functions.

MATERIALS AND METHODS

Site-Directed Mutagenesis. A mutation coding for β:Thr143Gly substitution was introduced into *TUB2* by oligonucleotide mutagenesis using the method of Kunkel et al. (*10*). *TUB2* was carried on the plasmid pCS3 (*11*), and the presence of the mutation was confirmed by dideoxy sequencing of candidate mutant plasmids using the Sequenase 2.0 DNA sequencing kit (United States Biochemical, Cleveland, OH). The plasmid bearing the mutated β-tubulin gene was termed pCS3-T143G.

Strains and Growth Media. The mutant strain of *S. cerevisiae* carrying the *tub2*-T143G mutated β-tubulin gene was designated YT143G and was derived from strain FY41 (Table 1; kindly provided by Dr. F. Winston). YT143G was constructed by fragment-mediated gene replacement of the wild-type genomic *TUB2* with the 4.9 kb *Sac1*−*Sph1* fragment from pCS3-T143G. In addition to the mutated β-tubulin gene, the *Sac1*−*Sph1* fragment also carried a *URA3* marker. Transformation of FY41 was carried out by a lithium acetate method (*12*) and transformants were selected on the basis of conversion to uracil prototrophy. Uracil prototrophes were then screened for the presence of the mutant sequence by polymerase chain reaction sequencing of genomic DNA using the Gibco BRL dsDNA cycle sequencing system (Life Technologies, Inc., Gaithersburg, MD).

Yeast strains were grown at 32 °C in YPD or SD supplemented with the appropriate metabolites (*13*). The *Escherichia coli* strains used for mutagenesis, CJ236 and MV1190 (BioRad, Richmond, CA), were grown at 37 °C in LB (1% bacto-tryptone, 0.5% bacto-yeast extract, 1% NaCl), ampicillin (50 μg/mL) was added to the growth medium to select for the inclusion of plasmids.

Isolation of Yeast Tubulin. Yeast tubulin was isolated from 60−80 L of stationary FY41 or YT143G cultures by the method of Davis et al. (*14*). The tubulin purity was routinely 75−90%, as determined by densitometric scanning of Coomassie blue stained SDS−PAGE gels with an LKB (Bromma, Sweden) Ultroscan XL laser densitometer. Protein concentrations were determined by Bradford assay, using bovine serum albumin as a standard.

Nucleotide-Binding Assays. Tubulin nucleotide-binding affinities were assayed by the equilibrium method of Hummel and Dreyer (*15*) as modified for tubulin (*16*). Briefly, 100 μg samples of tubulin in 100 μL of PEM1 (100 mM PIPES, 2 mM EGTA, and 1 mM MgSO$_4$; pH 6.8) were fractionated on Sephadex G-25 columns (22 × 1 cm) pre-equilibrated at 4 °C with PEM1 buffer, 10% glycerol, and [^{3}H]GTP (100 Ci/mol) or [^{3}H]GDP (100 Ci/mol) over a 10−1000 nM concentration range. For each nucleotide concentration, the radiolabel and tubulin concentrations were determined in 0.5

mL fractions eluting from the columns, which were then used to calculate the stoichiometry of the bound nucleotide. The data were plotted in the form of a Scatchard plot from which the equilibrium dissociation constants were determined by linear regression analysis.

To determine whether the 500 μM GTP used in the assembly-dependent GTPase assays (see the following discussion) was limiting for nucleotide binding to mutated tubulin, we took unassembled tubulin mixtures identical to those used for the GTPase assays, except that 500 μM [^{3}H]GTP was used in place of [γ^{32}P]GTP, and incubated the mixtures on ice for 30 min to allow for nucleotide exchange into the β-tubulin E site. The samples were then centrifuged through 1 mL Sephadex G-25 columns to remove the unbound label and to collect the eluants containing the bound nucleotide. The bound radiolabeled nucleotide and protein concentrations in the eluants were determined by scintillation counting and Bradford assays, respectively, from which we estimated the stoichiometry of nucleotide binding to the β-tubulin E site at 500 μM GTP.

Determination of Assembly-Dependent GTP Hydrolysis. The assembly-dependent GTP hydrolysis of MTs assembled from FY41 or YT143G tubulins was determined at polymer mass steady state as described by Davis et al. (*17*). Briefly, 100 μL aliquots of purified yeast tubulin at 1−2 mg/mL were incubated at 30 °C in PEM1 buffer, 10% glycerol, and 500 μM [γ^{32}P]GTP (75−150 Ci/mol). At timed intervals, 5 μL aliquots were quenched with 295 μL of 10% (v/v) acetic acid, 2.5 mM KH$_2$PO$_4$, and 10% (w/v) activated charcoal. The slurries were mixed by vortexing, and the charcoal-bound radiolabeled GTP was sedimented by centrifugation for 15 min in a microfuge. The amount of ^{32}P$_i$ released was then determined by scintillation counting of the supernatant. The data were corrected for background (nonassembly-dependent) GTPase activity by subtracting the GTPase activity of tubulin solutions under nonassembly conditions. We also corrected the steady-state hydrolysis rates for the number of microtubule ends, determined from the polymer mass steady state and the microtubule length measurements (*18*).

Measurement of MT Steady-State Dynamics in Vitro. Microtubules were visualized using video-enhanced differential interference contrast (VEDIC) microscopy at 30 °C as described by Sage et al. (*11*). MTs were assembled in PEM1 buffer containing 500 μM GTP at a tubulin concentration of 1−2 mg/mL. *Strongylocentrotus purpuratus* axonemes were used as "seeds" and were prepared by the method of Bell et al. (*19*) as modified by Walker et al. (*20*). The MT assembly mix was maintained at 30 ± 1 °C by a temperature-controlled stage and was viewed with a Zeiss IM35 microscope equipped with a Zeiss Planapo 63 × 1.4-na oil immersion objective. Background-subtracted images were obtained with a Newvicon (Hamamatsu c2400) video camera (Hamamatsu Photonics, Hamamatsu, Japan) and a Hamamatsu DVS-3000 image processor. Images were videotaped in super VHS format with a JVC (Tokyo, Japan) HRs5800u VCR for later analysis.

All of the measurements of MT time-dependent length changes were carried out between 35 and 70 min after initiation of assembly to ensure that the MTs were at steady state. MT length measurements were taken at 15−45 s intervals from the real-time video images using an IBM-

compatible computer equipped with a Targa-M8 frame grabber (Tru-vision, Corte Madera, CA) and JAVA video analysis software (Jandel Scientific, Sausalito, CA). The time-averaged growth rates (TAGRs) of individual MTs were determined from a linear regression analysis of the time-dependent length changes of each MT over the MT lifetime (the total observation time of an MT). A catastrophe was the sudden conversion of a growing MT to disassembly, which for wild-type MTs generally proceeded to completion, back to the axonemal seed. The MT disassembly rate was calculated from the length of MT disassembled and the time for the disassembly event. A conversion factor of 1695 subunits μm^{-1} of MT length was used in calculating both growing and disassembling rates.

Determination of Yeast Growth Rates. FY41 and YT143G cultures were grown overnight in SD media supplemented with the appropriate metabolites (*13*) and inoculated into fresh YPD media to an absorbance of 0.1 at 600 nM. Cell-doubling times were calculated from the increase in the turbidity over time for three cell doublings. Cell viability of the FY41 and YT143G strains during growth was assayed by plating known numbers of cells (determined by haemocy-tometry counting) onto YPD plates and counting the number of grown colonies after 7 days at 32 °C.

Measurement of MT Arrays in Cells. Aliquots of exponentially growing asynchronous cultures were fixed and stained as described previously (*21*). MTs were visualized by staining cells with the rat monoclonal anti-α-tubulin primary antibody, YOL1/34 (*22*; Sera Labs, Loughborough, U.K.), at a 1:400 dilution and a flourescein-conjugated goat anti-rat secondary antibody (Cappel, Durham, NC) at a 1:300 dilution. Cells were viewed with a Nikon Microphot microscope equipped with flourescence optics, and frame-averaged contrast enhanced images of random fields of cells were recorded with a Dage SIT video camera and Dage 2000 image processor. These images were then played back on a Sony (Tokyo, Japan) high-resolution monitor, and the lengths of MT structures in large-budded cells were measured using a Targa-M8 frame grabber (Tru-vision, Corte Madera, CA) and JAVA video analysis software (Jandel Scientific, Sausalito, CA).

Determination of Bud Morphology and Nuclear Position. Asynchronous, exponentially growing cells were stained with DAPI[1] at a concentration of 1 $\mu g/mL$ for 10 min. Photomicrographs of the cells were then obtained using a Zeiss PM III microscope and TMax-400 film, using both fluorescence and light microscopy. Nuclear position was determined in at least 450 large-budded cells (bud size of at least 75% of the mother cell size) for wild-type and YT143G cultures. The data given in Table 3 are average values, expressed as decimal fractions of the total observations for each culture.

Flow Cytometry. Cells used for flow cytometry were fixed in 70% ethanol overnight at 4 °C, washed in Tris buffer (50 mM Tris; pH 8), and then incubated in Tris buffer plus 1 mg/mL of RNase for 1 h at 37 °C. The cells were then pelleted, resuspended in 55 mM HCl containing 5 mg/mL pepsin, and incubated for 45 min at 37 °C. The cells

---

[1] Abbreviations: DAPI, 4′,6′-diamidino-2-phenylindole; EGTA, [ethylenebis(oxyethylenenitrilo)]tetraacetic acid; PIPES, 1,4-piperazinediethanesulfonic acid; SDS−PAGE, sodium dodecyl sulfate−polyacrylamide gel electrophoresis.

Table 2: Biochemical Properties of *tub2*-T143G Tubulin[a]

yeast *β*-tubulin genotype	K_D of Mg:GTP (nM)	microtubule GTPase (P_i min^{-1} MT^{-1})	microtubule growth rate ($\mu m\ h^{-1}$)	microtubule disassembly rate (s^{-1})
TUB2	61 ± 12	1500 ± 800	14.4 ± 1.7	3200 ± 300
tub2-T143G	>1000	100 ± 30	3.7 ± 1.4	not observed[b]

[a] GTP binding was assayed under equilibrium conditions using Hummel−Dreyer columns; the stoichiometry of GTP binding to the mutated tubulin was <0.1 mol of GTP/mol of tubulin dimer at 1000 nM, the highest GTP concentration practical with the method. The microtubule GTPase activity at 30 °C was determined at steady state and corrected for the number of microtubules; each value is the mean of four separate determinations. The microtubule growth and disassembly rates off plus-ends of flagellar axonemes were determined at steady state, using video microscopy. [b] The mutated microtubules were not observed to disassemble in over 4 h of accumulated observation time; with control microtubules, 16 disassembly events were observed in the same time period.

were again pelleted and resuspended in a propidium iodide solution (0.05 mg/mL in 0.18 M Tris (pH 7.5), 0.19 M NaCl, and 70 mM $MgCl_2$·$6H_2O$) overnight at 4 °C. Before analysis, 50 μL of the cells was diluted into 2 mL of Tris buffer and briefly sonicated to separate cells. Flow cytometry analysis was performed by Cytometry Sorting Specialists (La Jolla, CA) on a Becton-Dickinson FACScan (San Jose, CA).

RESULTS

YT143G Tubulin Has a Reduced Affinity for Guanine Nucleotide. It has been proposed that the glycine-rich peptide Gly-Gly-Gly-Thr-Gly-Ser-Gly contributes to the exchangeable GTP-binding site (E site) of *β* tubulin (*23*, *24*). To examine this possibility, we investigated the effects of a *tub2-T143G* mutation on nucleotide binding in vitro, using tubulin isolated from the haploid mutant YT143G (Table 1). The mutated tubulin consisted of heterodimers of wild-type α tubulin (*TUB1* and *TUB3* products) and mutated *β* tubulin expressed from *tub2-T143G*. Tubulin from wild-type yeast cells (FY41) was used as a control. Control tubulin heterodimers were composed of wild-type α tubulin and wild-type *β* tubulin (from *TUB2*). The equilibrium nucleotide-binding affinity for GTP was determined by the method of Hummel and Dreyer using a nucleotide concentration range of 10−1000 nM (see the Materials and Methods section).

GTP binding to the FY41 control tubulin in the presence of 1 mM $MgSO_4$ (K_D = 61 ± 12 nM; 0.9 mol/mol tubulin; Table 2) was comparable to that reported previously for wild-type yeast tubulin and vertebrate brain tubulin (*11*, *14*). No binding occurred in the absence of Mg^{2+}. In contrast with α*β*:Thr143Gly-mutated tubulin from YT143G cells, no Mg:GTP or Mg:GDP binding was detected at the lower nucleotide concentrations, and even at the highest nucleotide concentration of 1000 nM, the binding was only 0.05 mol/mol (Figure 1). Because of the specific radioactivity of the [^{3}H]GTP or [^{3}H]GDP used in the Hummel−Dryer columns (see the Materials and Methods section), a nucleotide concentration of 1000 nM was the practical limit of the Hummel−Dreyer method under our conditions.

In light of a report that a mutation within this region of another GTPase, *FtsZ*, increased the ATP-binding affinity (*9*), we also examined the ATP-binding affinity of YT143G

Table 3: Cell-Cycle Effects of the *tub2*-T143G *β*-Tubulin Mutation[a]

β-tubulin Genotype	2T (min)	Benomyl Sensitivity (µg/ml)	1C:2C	Bud Morphology			Nuclear Position		
TUB2	110	40	52:48	0.61	0.22	0.17	0.09	0.03	0.05
tub2-T143G	240	5	43:57	0.35	0.24	0.41	0.24	0.06	0.11

[a] 2T is the cell-doubling time in min, as determined in YPD liquid medium at 32 °C over three generations. The benomyl concentrations required to prevent cell growth were determined on YPD plates after 7 days of growth at 32 °C. The percentages of cells with unreplicated (1C) and replicated (2C) DNA were determined by flow cytometry (see the Materials and Methods section). The bud morphology and nuclear position were determined in asynchronous, exponentially growing cultures by light and fluorescence microscopy, after staining the cells with DAPI. The nuclear position was determined in large-budded cells (bud size at least 75% of mother cell size). At least 450 cells were examined for each culture, and the data are presented as average values, expressed as decimal fractions of the total observations for each culture. The time required to complete nuclear segregation (see Discussion) was calculated from the product of the cell-doubling time and the proportion of large-budded cells with unsegregated nuclei ($110 \times 0.12 = 13$ min for wild-type cells and $240 \times 0.30 = 80$ min for mutant cells).
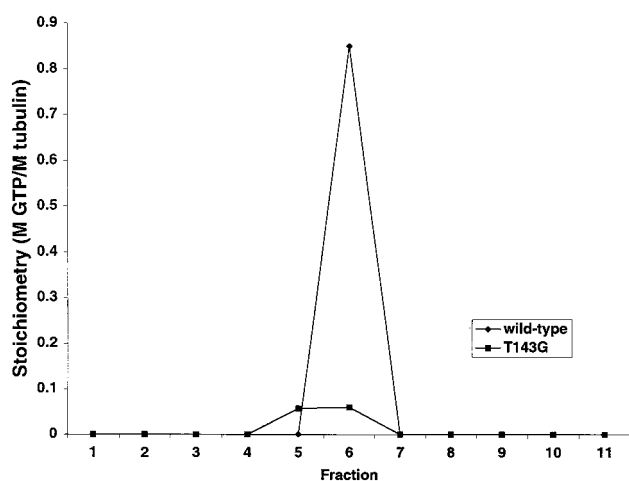

FIGURE 1: Determination of tubulin nucleotide-binding affinity by the equilibrium method of Hummel and Dreyer (*15*). The 100 µg samples of tubulin from wild-type (FY41) and mutant (YT143G) cells were fractionated over Sephadex G-25 columns equilibrated with $10-1000$ nM [³H]GTP (100 Ci/mmol) at 4 °C. The stoichiometry of GTP binding to the tubulin was determined from the radionucleotide and tubulin concentrations in 0.5 mL fractions eluting from the columns. The binding stoichiometries were graphed as a function of the free GTP concentration in a Scatchard plot from which the equilibrium binding constant was determined. In the above graph, the elution profile of tubulin isolated from wild-type cells (◆) and YT143G mutant cells (■) is shown for the 1000 nM GTP concentration, the highest concentration possible under the experimental conditions. Note that, even at this GTP concentration, little binding to the YT143G tubulin was detected.
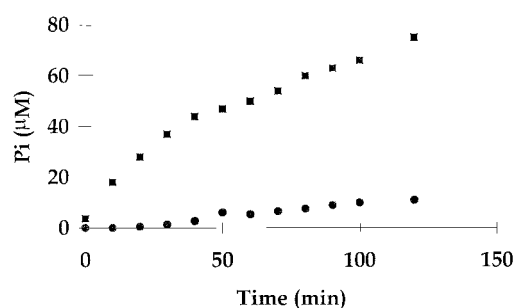

FIGURE 2: Polymerization-dependent GTP hydrolysis by tubulin from wild-type (FY41) and mutant (YT143G) haploid cells. MT polymerization was initiated in tubulin solutions ($1-2$ mg/mL) in PEM1 buffer containing 500 µM GTP by incubation at 30 °C. At timed intervals, 5 µL aliquots of the MT suspensions were quenched in 295 µL of a charcoal suspension to assay radiolabeled P_i release (see the Materials and Methods section). Nonpolymerization-dependent GTP hydrolysis was determined in duplicate samples maintained at 4 °C and was subtracted from the corresponding experimental value. The steady-state rates of GTP hydrolysis reported in Table 2 were determined by linear regression analysis using data points between 40 and 120 min after assembly initiation and were corrected for the number of MT ends (see the Materials and Methods section). To ascertain that polymer mass steady state was achieved, MT aliquots were taken at 40 and 120 min and sedimented, and the polymer mass in the pellets was determined by Bradford assay. MT lengths at these times were also determined from electron microscopic examination of fixed MT aliquots and were used to calculate the number of MT ends (see the Materials and Methods section). In the experiment shown, the MT number concentrations and steady-state hydrolysis rates were calculated to be 0.55 nM and 700 P_i/min/MT for wild-type MTs (■) and 1.0 nM and 50 P_i/min/MT for mutated MTs (●).

mutated tubulin. In contrast to the *FtsZ* result, however, there was no detectable increase in the ATP-binding affinity of YT143G tubulin over that of wild-type yeast tubulin ($K_D > 1000$ nM for both tubulins; data not shown).

YT143G Tubulin Has Reduced Assembly-Dependent GTPase Activity. We examined whether *β*:Thr143 plays a role in GTP hydrolysis by *β* tubulin by assaying the assembly-dependent GTPase activity of MTs assembled in vitro using tubulin isolated from YT143G mutant cultures. Tubulin isolated from wild-type cultures was used as a control. The tubulins were assembled to polymer mass steady state at 30 °C in the presence of 500 µM [γ³²P]GTP, and the rates of GTP hydrolysis were determined at steady state from the release of ³²P_i. The ³²P_i release data were corrected both for

the nonassembly-dependent hydrolysis of GTP and for the number of MT ends (see the Materials and Methods section). As shown in Figure 2 and Table 2, the steady-state GTPase activity of the control MTs (1500 ± 800 P_i/min/MT) was comparable to that obtained previously for tubulin isolated from wild-type cells (*14*). In contrast, the steady-state GTPase activity of MTs assembled from YT143G tubulin (100 ± 30 P_i/min/MT) was approximately 15-fold lower than that of the control MTs.

We tested whether the lower GTPase activity of the mutated MTs was simply a result of the lower GTP-binding affinity of the YT143G tubulin, which could result in fewer

MT subunits with bound nucleotide. To do this, control and mutated tubulins were incubated with 500 μM [^{3}H]GTP (the same nucleotide concentration as that used in the assembly-dependent GTPase assays), and the tubulin−nucleotide complexes were centrifuged through Sephadex G25 columns to remove the unbound radionucleotide. The stoichiometry of the tubulin-bound nucleotide was then calculated in samples of eluted tubulin (see the Materials and Methods section). Although the GTP-binding stoichiometry of the mutated β tubulin was somewhat lower than that of control tubulin (0.5 ± 0.12 versus 0.9 ± 0.24 mol/mol for control tubulin), the difference appears to be too small to account for the 15-fold lower assembly-dependent GTPase activity of the mutated tubulin. Thus, the slower GTPase activity of the mutated MTs cannot result solely from a lower stoichiometry of GTP binding to the mutated subunits.

YT143G Tubulin Suppresses MT Assembly and Disassembly in Vitro. In light of the effect of the *tub2-T143G* mutation on assembly-dependent tubulin GTPase activity and of the proposed role of GTP hydrolysis in MT growing and shortening dynamics (*2*, *25*), we examined whether the mutation also affected the dynamic properties of individual MTs in vitro using VEDIC microscopy (see the Materials and Methods section).

As observed previously, wild-type yeast MTs grew at a much slower rate than vertebrate brain MTs, they did not exhibit the large length excursions typical of brain MTs, and they exhibited a far lower rescue frequency. Under steady-state conditions, control tubulin isolated from wild-type cells assembled into MTs that grew continuously at an average rate of 14.4 ± 1.7 μm/h until they underwent a switch to disassembly, which usually proceeded to completion at an average rate of 3200 ± 300 dimers/s (Figure 3a and Table 2). Both the growing and shortening rates of the wild-type MTs were comparable to those previously reported (*11*). By comparison, the average steady-state growth rate of individual MTs assembled from YT143G mutant tubulin was 4-fold slower than that of control MTs (3.7 ± 1.4 versus 14.4 ± 0.8 μm/h; Figure 3 and Table 2). This was clearly seen in the shift to slower rates of the TAGR distribution for individual mutated MTs (Figure 3c).

Some heterogeneity in the TAGRs of both control and mutated MTs was evident; a small number of control MTs grew very slowly, while some mutated MTs grew at rates approximating the average control rate (Figure 3c). A similar heterogeneity in the in vitro growing (and shortening) rates has been reported for bovine MTs (*26*). On the basis of studies with the nonhydrolyzable GTP analogue, GMPPCP, it was concluded that the growth rate variability was intrinsic to MTs but that it occurred independently of MT dynamic instability and probably did not involve E-site GTP hydrolysis (*27*). It is possible, therefore, that the growth-rate distributions shown in Figure 3c reflect this intrinsic variability. Nevertheless, the distinct shift in the TAGR distributions for YT143G and FY41 MTs indicate that the *tub2-T143G* mutation results in MTs with markedly slower growing rates.

Moreover, in over 4 h of observation, we never observed a disassembly event with the mutated MTs (e.g., Figure 3b), which places an upper limit for the growing-to-shortening transition frequency at approximately $1/(4 \times 60 \times 60) = 0.00007$ s^{-1}. During the same amount of observation
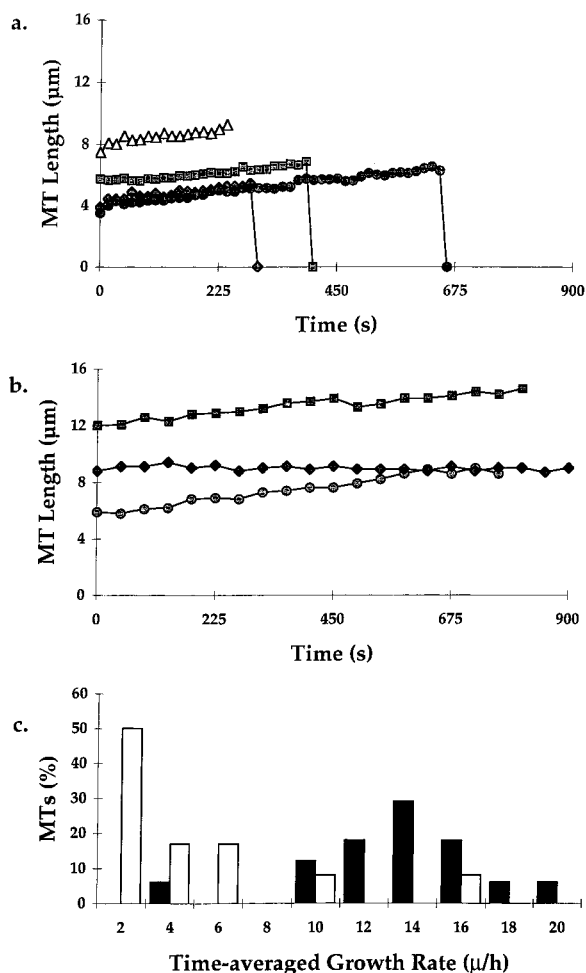

FIGURE 3: In vitro MT dynamic properties measured by VEDIC microscopy. MTs were assembled to steady state at 30 °C in PEM1 buffer containing 500 μM GTP from (a) FY41 wild-type tubulin and (b) YT143G mutant tubulin. The initial tubulin concentrations were 1 mg/mL for both samples. Time-dependent length changes of the MTs were determined every 15−45 s (see the Materials and Methods section), and plots for individual MTs from each tubulin sample are shown. The TAGRs given in Table 2 were determined from such plots by a linear regression analysis of MT growth over the lifetime of an individual MT. Occasionally, an MT would disappear from the plane of focus before undergoing disassembly (a, Δ). In these instances, the regression analysis was carried out over the available data. (c) The distributions of the TAGRs for 25 individual MTs assembled from wild-type (shaded) and mutated (unshaded) tubulins.

time with control MTs, 16 MTs underwent transitions to disassembly, corresponding to a growing-to-shortening transition frequency of 0.0012 s^{-1}, which was comparable to our earlier results (*11*, *14*). The disassembly transition frequency of MTs assembled from YT143G tubulin was, therefore, at least 15-fold slower than that of control MTs. Thus, MTs assembled from the mutated tubulin not only have significantly slower growing rates, but also their disassembly is suppressed.

Effects of tub2-T143G on MTs in Cells. By immunofluorescence microscopy, the spindles in YT143G mutant cells appeared shorter than those in large-budded wild-type cells (cf. parts a and b of Figure 4). This was confirmed by quantifying spindle lengths in large-budded cells from asynchronous, exponentially growing cultures (Figure 4c). The average spindle length in large-budded wild-type cells
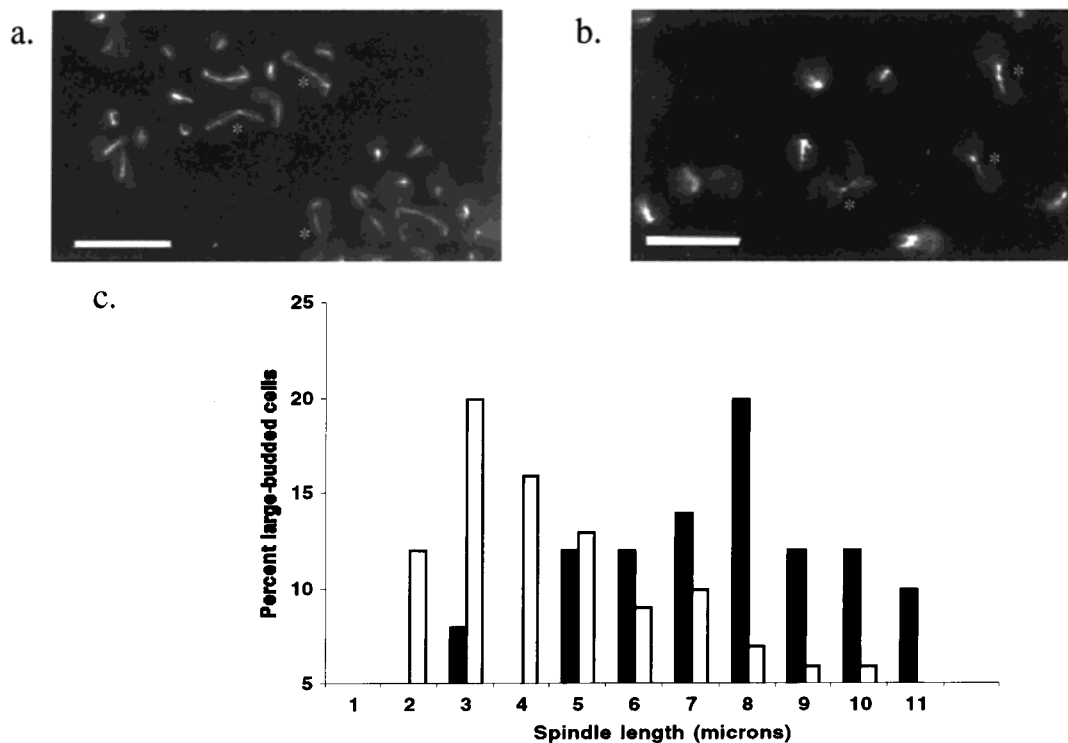
FIGURE 4: MT arrays in (a) FY41 wild-type and (b) YT143G mutant cells. MT arrays in asynchronous, exponentially growing cultures were visualized using a monoclonal anti-α-tubulin antibody and quantified by immunofluorescence microscopy (see the Materials and Methods section). Examples of large-budded cells in both wild-type and mutant cultures are marked with an asterisk. Note the smaller size of the MT arrays in large-budded YT143G cells when compared with those in large-budded wild-type cells. Notice also that the spindles in large-budded mutants cells, though short, can still reach across the bud neck (two cells, right side of the panel in part b). Legend bar = 10 μm. (c) The lengths of MT arrays in at least 100 large-budded cells were measured for FY41 wild-type (shaded) and YT143G mutant (unshaded) cultures and plotted as a histogram.

was 7.1 ± 0.4 μm, consistent with earlier measurements of late anaphase spindles (*28, 29*). In contrast, the average spindle length was only 3.7 ± 0.2 μm in large-budded mutant cells, suggesting a delay in initiating or carrying out anaphase. In light of the slower in vitro growth rates of mutated MTs, one explanation for this phenotype is that spindle MT assembly may be slower in the YT143G mutant cells, thus slowing mitosis. Alternatively, the transition from metaphase to anaphase may be delayed.

Support for these arguments came from comparing the cell-cycle properties of asynchronous, exponentially growing wild-type and mutant cultures (Table 3). First, the doubling time of mutant cultures was 240 min, approximately twice as long as that of wild-type cultures. This increased doubling time did not occur because the mutant cultures had a lower viability rate; viability studies (see the Materials and Methods section) showed the mutant and wild-type cultures to have essentially the same proportion of viable cells during the three doublings over which the measurements were made (data not shown).

Second, asynchronous mutant cultures contained higher proportions both of large-budded cells (41% versus 17% for wild-type) and of large-budded cells with unsegregated nuclei (30% versus 12% for wild-type). Flow cytometric analyses also showed that mutant cultures had a greater proportion of cells with replicated DNA that had not undergone cell division (column 1C:2C in Table 3). These results indicated that nuclear segregation was significantly slower in mutant cells, and from the cell-doubling time and morphology data in Table 3, we calculated that it took over 6 times longer to

complete nuclear segregation in mutant cells (80 versus 13 min for wild-type cells; see legend in Table 3).

DISCUSSION

Implications for the β-Tubulin GTP-Binding Site and the GTPase Superfamily. The biochemical effects of the *tub2-T143G* mutation on tubulin and MTs indicate that β: Thr143 plays an important role in E-site GTP binding and hydrolysis. Both the GTP-binding affinity and the MT-dependent GTP hydrolysis rate were markedly reduced for dimers carrying the Thr143Gly-mutated β tubulin, when compared with control dimers. Comparable effects on nucleotide binding have also been seen for mutations in the cognate sequences of ATPases and GTPases, including the bacterial GTPase, FtsZ (*6, 7, 9, 30−32*). In a recent electron crystallographic model of the tubulin dimer (down to a 3.7 Å resolution), the glycine-rich tubulin signature motif Gly-Gly-Gly-Thr-Gly-Ser-Gly is located near the phosphates of the E-site nucleotide (*5*). Similar glycine-rich sequences lie very close to the phosphates of the bound nucleotide in X-ray crystallographic models of ATPases (*6, 7*) and the bacterial GTPase, FtsZ (*33*). It is probable, therefore, that β: Thr143 contributes to the GTP-binding E site and may even play a direct role in the catalytic mechanism.

The results support the idea that the tubulins are a structurally distinct family within the GTPase superfamily. It has been pointed out (e.g., refs *24* and *34*) that none of the primary sequences of the α, β, and γ tubulins exhibit the motifs that contribute to the guanine nucleotide binding

site in classic or conventional GTPases, such as p21[ras] and EF-Tu (e.g., refs *4, 35,* and *36*). Even though the tubulins and many other GTPases have a Rossman fold topology in common, members of the GTPase superfamily can differ significantly from one another with respect both to their primary sequences and to the details of nucleotide binding. In the α and β tubulins, for example, two loops (one containing the tubulin signature motif) "sandwich" the phosphates of the bound nucleotide; in p21[ras] or EF-Tu, by contrast, a single P loop appears to perform this role (*5*). Another GTPase, FtsZ, shows strong structural similarities with the tubulins (*33*), and it has been suggested that it is an evolutionary precursor of the tubulins (*37*) and belongs in the tubulin family of GTPases (*38*), despite there being limited primary sequence identity with the tubulins. Thus, the tubulins and FtsZ, when compared with classic GTPases, appear to represent a parallel evolutionary solution to the GTP-binding problem.

Role of the β-Tubulin GTPase in MT Dynamics. MTs assembled from αβ:Thr143Gly tubulin have clearly suppressed dynamics in vitro. First, the MT steady-state growing rate is reduced ca. 4-fold as compared with control MTs (Table 2). Second, we did not observe any of the αβ:Thr143Gly MTs to undergo a transition from growing to disassembling in over 4 h of observation (e.g., Figure 3b). This implies that the maximum value for the disassembly transition frequency for αβ:Thr143Gly MTs is approximately $1/(4 \times 60 \times 60) = 0.00007$ s^{-1}, at least 15-fold lower than the corresponding frequency for control MTs (ca. 0.0011 s^{-1}). In related work (*39*), we showed that MTs assembled from αβ:Thr143Gly tubulin contained far higher stoichiometries of both E-site GTP (819 versus 173 MT^{-1} for control MTs) and GDP + P$_i$ (3924 versus 248 MT^{-1} for control MTs). Together, the results support the "cap" hypothesis in which it was proposed that tubulin subunits with GTP or GDP + P$_i$ bound in the E sites stabilize an MT end from disassembly (*2, 25*).

The slower steady-state growth rate of the mutated microtubules was unexpected because the hydrolysis of E-site GTP is clearly uncoupled from tubulin−GTP addition to yeast MT ends (*39*; see also refs *25* and *40*). Because the two reactions are uncoupled, the MT growth rate should be independent of the GTP hydrolysis rate; instead we found that the slower GTP hydrolysis rate of the mutated MTs was associated with a slower MT growth rate (Table 2). One possible explanation is suggested by our earlier observation that the β:Thr143Gly-containing MTs have far higher E-site GTP and GDP + P$_i$ contents than control MTs (*39*). If an MT end becomes saturated with tubulin−GTP subunits (i.e., all of the available elongation sites at the MT end are occupied by tubulin−GTP dimers), then the MT end would no longer be at a steady state (treadmilling; *1*) but would be in equilibrium with the tubulin−GTP subunits in solution. As a result, MT growth would stall, unless further E-site GTP hydrolysis or P$_i$ release regenerated new elongation sites. By this argument, the slower growth rate of αβ:Thr143Gly MTs arises because the slower GTPase activity more slowly regenerates new assembly sites for further subunit addition, leading to a tubulin−GTP-saturated MT end. This is similar to the "lateral cap" model, which treats MT elongation as a function of the nucleotide composition of neighboring subunits at the MT end (*41*), and such a model

does not preclude an uncoupled mechanism for the tubulin−GTP addition and hydrolysis reactions.

Regardless of the mechanism, the data show that the *tub2-T143G* mutation results in slower growing, more stable MTs in vitro, and this is consistent with the effects of the mutation in cells: a delay in mitosis. The average spindle length in large-budded mutant cells was only 3.7 ± 0.2 μm, approximately half of the average length of spindles in large-budded wild-type cells (7.1 ± 0.4 μm; Figure 4), suggesting a delay between metaphase and completion of anaphase. Asynchronous mutant cultures also exhibit a higher proportion of cells that have not yet completed nuclear segregation when compared to wild-type cells (Table 3), again indicating that there is such a delay. One explanation for the delay is that the mutation suppresses spindle MT dynamics, similar to the effects of the mutation on MTs in vitro, and slows the rate of spindle MT elongation. Support for this idea is given by the recent demonstration that MTs in yeast cells, like their counterparts in higher eukaryotes, are dynamic and grow and shorten from their (+) ends throughout mitosis (*42, 43*). However, if the *tub2-T143G* mutation does affect spindle MT dynamics, this could also lead to other lesions, which would delay the onset of anaphase.

It also appears that there is a delay in nuclear positioning to the bud neck in cells containing the tubulin mutation (Table 3). This would suggest a defect in cytoplasmic MT function as well. For example, cytoplasmic MTs with suppressed dynamics could have a lower probability of capture by the Kar9p and dynein−dynactin complexes, which contribute to spindle orientation and migration to the bud neck (*44−46*). Indeed, the delayed nuclear migration in YT143G mutant cells is reminiscent of the phenotype of cells that lack Bim1p, a protein necessary for MT−Kar9p interaction (*47*). We did not, however, see the dramatic changes in astral MT length distribution that were observed when some microtubule-motor proteins are deleted [e.g., a kip3 deletion results in longer astral MTs while a kip2 deletion results in shorter astral MTs, as compared to wild-type cells (*48*)]. This could be due to the specific dynamic parameters affected by the T143 tubulin mutation as compared to those affected by MT-interacting proteins. Alternatively MT-interacting proteins in the cell may compensate, to some extent, for the tubulin defect.

The slower nuclear segregation does not lead to binucleate cells or cell death, presumably because the "checkpoint" pathways can "sense" both when the spindle has entered the emerging bud (*49−51*) and defects within the spindle itself (*52−54*). These checkpoint pathways delay cell-cycle progression until the defect is corrected (e.g., refs *53* and *54*). Indeed, even though the spindles are shorter in large-budded mutant cells, in at least some cells, the spindles are long enough to reach across the bud neck (Figure 4b). Thus, it is reasonable to think that these shorter spindles allow for the completion of nuclear segregation, albeit more slowly than in wild-type cells, and that checkpoint pathways delay the onset of cytokinesis.

On the basis of the biochemical and phenotypic effects of the *tub2-T143G* mutation, it is reasonable to think that the mutation slows MT assembly in mutant cells by reducing the MT-associated GTPase activity and that this leads to the slowing of nuclear migration and to a longer mitosis. By extrapolation, the data further suggest that MT assembly

Dougherty et al.

during the normal cell cycle could be slowed or even stalled by reducing β-tubulin GTPase activity. In the past few years, many new factors have been discovered that influence MT dynamics during the cell cycle (e.g., ref *55*). One such factor could be part of a control pathway that regulates the β-tubulin GTPase activity and coordinates MT assembly with other cell-cycle events.

ACKNOWLEDGMENT

REFERENCES

1. Margolis, R., and Wilson, L. (1978) *Cell 13,* 1−8.
2. Mitchison, T., and Kirschner, M. (1984) *Nature 312*, 237−242.
3. Gelfand, V. I., and Bershadsky, A. D. (1991) *Annu. Rev. Cell Biol. 7*, 93−116.
4. Dever, T. E., Glynias, M. J., and Merrick, W. C. (1987) *Proc. Natl. Acad. Sci. U.S.A. 84*, 1814−1818.
5. Nogales, E., Wolf, S. G., and Downing, K. H. (1998) *Nature 391*, 199−203.
6. Reinstein, J., Brune, M., and Wittinghofer, A. (1988) *Biochemistry 27*, 4712−4720.
7. Reinstein, J., Schlichting, I., and Wittinghofer, A. (1990) *Biochemistry 29*, 7451−7459.
8. RayChaudhuri, D., and Park, J. T. (1992) *Nature 359,* 251−254.
9. RayChaudhuri, D., and Park, J. T. (1994) *J. Biol. Chem. 269*, 22941−22944.
10. Kunkel, T. A., Roberts, J. D., and Zakour, R. A. (1987) *Methods Enzymol. 154*, 367−382.
11. Sage, C. R., Davis, A. S., Dougherty, C. A., Sullivan, K., and Farrell, K. W. (1995) *Cell Motil. Cytoskeleton 30,* 285−300.
12. Ito, H., Fukuda, Y., Murata, K., and Kimura, A. (1983) *J. Bacteriol. 153*, 163−168.
13. Sherman, F., Fink, G. R., and Hicks, J. B. (1986) Laboratory Course Manual for Methods in Yeast Genetics. *Cold Spring Harbor,* Cold Spring Harbor Laboratory, Plainview, NY.
14. Davis, A., Sage, C. R., Wilson, L., and Farrell, K. W. (1993) *Biochemistry 32*, 8823−8835.
15. Hummel, J. P., and Dreyer, W. J. (1962) *Biochim. Biophys. Acta 63*, 530−532.
16. Seeberg, P. H., Colby, W. W., Capon, D. J., Goedel, D. V., and Levinson, A. D. (1984) *Nature 312*, 71−75.
17. Davis, A., Sage, C. R., Dougherty, C. A., and Farrell, K. W. (1994) *Science 264*, 839−842.
18. Farrell, K. W., Jordan, M. A., Miller, H. P., and Wilson, L. (1987) *J. Cell Biol. 104*, 1035−1046.
19. Bell, C. W., Fraser, C., Sale, W. S., Tang, W. J., and Gibbons, I. R. (1982) *Methods Cell Biol. 24*, 373−397.
20. Walker, R. A., O'Brien, E. T., Pryer, N. K., Soboeiro, M. F., Voter, W. A., and Erickson, H. P. (1988) *J. Cell Biol. 107*, 1437−1448.
21. Adams, A. E., and Pringle, J. R. (1984) *J. Cell Biol. 98*, 934−935.
22. Kilmartin, J. V., Wright, B., and Milstein, C. (1982) *J. Cell Biol. 93*, 576−582.
23. Mandelkow, E. M., Herrmann, M., and Ruhl, U. (1985) *J. Mol. Biol. 185*, 311−327.
24. Sternlicht, H., Yaffe, M. B., and Farr, G. W. (1987) *FEBS Lett. 214*, 226−235.
25. Carlier, M. F., and Pantaloni, D. (1981) *Biochemistry 20*, 1918−1924.
26. Gildersleeve, R. F., Cross, A. R., Cullen, K. E., Fagen, A. P., and Williams, R. C., Jr. (1992) *J. Biol. Chem. 267*, 7995−8006.
27. Dye, R. B., and Williams, R. C., Jr. (1996) *Biochemistry 35*, 14331−14339.
28. Palmer, R. E., Koval, M., and Koshland, D. (1989) *J. Cell Biol. 109*, 3355−3366.
29. Yeh, E., Skibbens, R. V., Cheng, J. W., Salmon, E. D., and Bloom, K. (1995) *J. Cell Biol. 130*, 687−700.
30. Neal, S. E., Eccleston, J. F., Hall, A., and Webb, M. R. (1988) *J. Biol. Chem. 263*, 19718−19722.
31. Krab, I. M., and Parmeggiani, A. (1999) *Biochemistry 38*, 13035−13041.
32. Pieper, U., Schweitzer, T., Groll, D. H., Gast, F. U., and Pingoud, A. (1999) *J. Mol. Biol. 292*, 547−556.
33. Lowe, J., and Amos, L. A. (1998) *Nature 391,* 203−206.
34. Burns, R. G., and Farrell, K. W. (1996) *Trends Cell Biol. 6*, 297−303.
35. Bourne, H. R., Sanders, D. A., and McCormick, F. (1991) *Nature 349*, 117−127.
36. Valencia, A., Chardin, P., Wittinghofer, A., and Sander, C. (1991) *Biochemistry 30*, 4637−4648.
37. Erickson, H. (1995) *Cell 80*, 367−370.
38. Nogales, E., Downing, K. H., Amos, L. A., and Lowe, J. (1998) *Nat. Struct. Biol. 5*, 451−458.
39. Dougherty, C. A., Himes, R. H., Wilson, L., and Farrell, K. W. (1998) *Biochemistry 37*, 10861−10865.
40. Burns, R. G. (1991) *Biochem. J. 277*, 239−243.
41. Bayley, P. M., Schilstra, M. J., and Martin, S. R. (1990) *J. Cell Sci. 95*, 33−48.
42. Pearson, C. G., Maddox, P. S., Salmon, E. D., and Bloom, K. (2001) *J. Cell Biol. 152*, 1255−1266.
43. Maddox, P. S., Bloom, K. S., and Salmon, E. D. (2000) *Nat. Cell Biol. 2*, 36−41.
44. Lee, L., Tirnauer, J. S., Li, J., Schuyler, S. C., Liu, J. Y., and Pellman, D. (2000) *Science 287*, 2260−2262.
45. Korineck, W. S., Copeland, M. J., Chaudhuri, A., and Chant, J. (2000) *Science 287*, 2257−2259.
46. Carminati, J. L., and Stearns, T. (1997) *J. Cell Biol. 138,* 629−641.
47. Miller, R. K., Cheng, S. C., and Rose, M. D. (2000) *Mol. Biol. Cell 11*, 2949−2959.
48. Cottingham, F. R., and Hoyt, M. A. (1997) *J. Cell Biol. 138*, 1041−1053.
49. Pereira, G., Hofken, T., Grindlay, J., Manson, C., and Schiebel, E. (2000) *Mol. Cells 6*, 1−10.
50. Bloecher, A., Venturi, G. M., and Tatchell, K. *Nat. Cell Biol. 2*, 556−558.
51. Li, R. (1999) *Proc. Natl. Acad. Sci. U.S.A. 96*, 4989−4994.
52. Pangilinan, F., and Spencer, F. (1996) *Mol. Biol. Cell 7,* 1195−1208.
53. Hoyt, M. A., Totis, L., and Roberts, B. T. (1991) *Cell 66*, 507−517.
54. Li, R., and Murray, A. W. (1991) *Cell 66*, 519−531.
55. Cassimeris, L. (1999) *Curr. Opin. Cell Biol. 11*, 134−141.